Article

Surface and tropospheric ozone trends in the Southern Hemisphere since 1990: possible linkages to poleward expansion of the Hadley Circulation

Xiao Lu[1,2], Lin Zhang[1*], Yuanhong Zhao[1], Daniel J. Jacob[2,3*], Yongyun Hu[1*], Lu Hu[4], Meng Gao[2], Xiong Liu[5], Irina Petropavlovskikh[6], Audra McClure-Begley[6], Richard Querel[7]

1 Laboratory for Climate and Ocean-Atmosphere Studies, Department of Atmospheric and Oceanic Sciences, School of Physics, Peking University, Beijing 100871, China

2 School of Engineering and Applied Sciences, Harvard University, Cambridge, MA 02138, USA.

3 Department of Earth and Planetary Science, Harvard University, Cambridge, MA 02138, USA.

4 Department of Chemistry and Biochemistry, University of Montana, Missoula, MT 59812, USA.

5 Harvard-Smithsonian Center for Astrophysics, Cambridge, MA 02138, USA.

6 Cooperative Institute for Research in Environmental Sciences, University of Colorado, Boulder, USA; NOAA Earth System Research Laboratory, Boulder, CO 80305, USA.

7 National Institute of Water and Atmospheric Research (NIWA), Lauder 9377, New Zealand.

Received 2018-11-22, received in revised form 2018-12-12, accepted 2018-12-14

Correspondence to: Lin Zhang (zhanglg@pku.edu.cn), Daniel J. Jacob (djacob@fas.harvard.edu), Yongyun Hu (yyhu@pku.edu.cn)

Abstract

Increases in free tropospheric ozone over the past two decades are mainly in the Northern Hemisphere that have been widely documented, while ozone trends in the Southern Hemisphere (SH) remain largely unexplained. Here we first show that in-situ and satellite observations document increases of tropospheric ozone in the SH over 1990-2015. We then use a global chemical transport model to diagnose drivers of these trends. We find that increases of anthropogenic emissions (including methane) are not the most significant contributors. Instead, we explain the trend as due to changes in meteorology, and particularly in transport patterns. We propose a possible linkage of the ozone increases to meridional transport pattern shifts driven by poleward expansion of the SH Hadley circulation (SHHC). The SHHC poleward expansion allows more downward transport of ozone from the stratosphere to the troposphere at higher latitudes, and also enhances tropospheric ozone production through stronger lifting of tropical ozone precursors to the upper troposphere. These together may lead to increasing tropospheric ozone in the extratropical SH, particularly in the middle/upper troposphere and in austral autumn. Poleward expansion of the Hadley circulation is partly driven by greenhouse warming, and the associated increase in tropospheric ozone potentially provides a positive climate feedback amplifying the warming that merits further quantification.

Keywords:

Tropospheric ozone, ozone trend, Southern Hemisphere, Hadley Circulation poleward expansion, widening of the tropics

1. Introduction

Tropospheric ozone is a major air pollutant and also an important short-lived greenhouse gas [1]. It is produced by photochemical oxidation of carbon monoxide (CO) and hydrocarbons in the presence of nitrogen oxides (NO_x), and is also transported downward from the stratosphere. It has a lifetime of a few weeks against chemical loss in the troposphere, sufficiently short that ozone budgets in the two hemispheres are largely independent. Free tropospheric ozone observations in the Northern Hemisphere (NH) since the 1980s show increasing trends that can be explained by anthropogenic emissions [2, 3] and modulation by climate variability [4, 5]. The Southern Hemisphere (SH) has much lower anthropogenic influence, yet most published studies using observations from surface sites, ozonesondes, and satellite instruments have recorded increasing tropospheric ozone since the 1990s [2, 6-8] (see also section 3). Previous analyses of individual ground and ozonesonde observations suggested that interannual variability of tropospheric ozone in the tropical and subtropical SH might be impacted by changes in anthropogenic emissions [3, 9], stratospheric intrusions [10-12], and the El Niño–Southern Oscillation (ENSO) [13]. However, causes of the large-scale increasing trends in the SH, remain largely unexplored. Current chemistry–climate models do not reproduce the observed trends in tropospheric ozone over the SH [2, 7, 14].

In this study, we first present observational evidence of increasing tropospheric ozone in the SH since 1990 derived from available surface, ozonesonde, and satellite observations. Factors contributing to the tropospheric ozone increases are then quantified using a set of simulations by a state-of-art global chemical transport model (GEOS-Chem) driven by assimilated meteorological data. We will show that climate change, particularly the shift of meridional transport, rather than increases in ozone precursor emissions, is the dominant factor controlling the trend of SH tropospheric ozone. We propose a previously unrecognized linkage of the SH tropospheric ozone increases with poleward expansion of the Hadley circulation through modulating the stratosphere-to-troposphere ozone transport and ozone chemical production in the upper troposphere. We will also discuss other possible drivers (e.g. regional warming, ENSO, stratospheric ozone recovery and circulation changes) in modulating the regional ozone trend in SH. Conclusions and implications are presented in Section 4.

2. Materials and methods

2.1 Ground and ozonesonde observations

We summarize here available in situ measurements of tropospheric ozone at locations that have more than 15-year valid records over the period of 1990–2015 in the SH. Hourly surface ozone measurements are assessed from the World Data Center of Greenhouse Gas (WDCGG; https://gaw.kishou.go.jp/, with monthly data available from the Tropospheric Ozone Assessment Report (TOAR) at https://doi.org/10.1594/PANGAEA.876108) and contributed by McClure-Begley et al. [15]. In order to derive a statistically robust trend, we apply the following criteria to select the sites: (1) have at least 18 hourly observations per day for calculating the daily mean. (2) have at least 18 daily observations per month for calculating the monthly mean. (3) have at least 2 monthly observations for calculating the seasonal mean, and at least 8 months for the annual mean. (4) have at least 16 annual mean observations for the period of 1990–2015. Nine surface sites in the SH meet these criteria and are used for our trend analyses as listed in Table S1 (online).

We also obtain ozonesonde measurements from the World Ozone and Ultraviolet Radiation Data Centre (WOUDC; http://woudc.org/data.php). WOUDC is operated by the Meteorological Service of Canada and includes 150 sites globally with 42 of them located in the SH. It includes sites from the Southern Hemisphere Additional Ozonesondes (SHADOZ) network, established in 1998 [16]. A recent work found that a sampling frequency of four sondes per month is needed to capture the interannual variability of ozone in the upper troposphere [10]. Here similar to the surface sites, we apply the following criteria for selecting the ozonesonde sites that have: (1) at least 4 observations per month for calculating the monthly mean; (2) at least 2 monthly observations for the seasonal mean, and at least 8 months for the annual mean; (3) at least 16 annual mean observations for the 1990–2015 trend estimation.

Two ozonesonde sites are then selected in this study (Table S1 online). The SHADOZ sites are not used here due to the late establishment.

2.2. Satellite observations

We also analyze two satellite products of tropospheric column ozone (TCO): the GOME-OMI

observations and OMI/MLS observations. GOME-OMI TCO is derived from the Global Ozone Monitoring Experiment (GOME, from July 1995–June 2003) and the NASA Earth Observing System (EOS) Aura satellite's Ozone Monitoring Instrument (OMI, October 2004–December 2015). Here we use the GOME (data available at https://www.cfa.harvard.edu/~xliu/res/gmtrop.htm) and OMI PROFOZ ozone profiles with 24 layers extending from surface to 60 km retrieved based on optimal estimation techniques [17]. TCO is derived using the NCEP daily tropopause height (defined by the 2 K km^{-1} lapse-rate metric). We combine the monthly gridded data at global 2°×2.5° horizontal resolution from GOME and OMI to obtain an approximately 20-year time-series covering 1996–2015 with a 15-month gap in 2003–2004, following the Tropospheric Ozone Assessment Report (TOAR) [8]. We do not include GOME data prior to March 1996 as it shows a high bias due to the use of a shorter integration time.

The OMI-MLS TCO product is derived from the combination of total column ozone observations from OMI and stratospheric column ozone observations from Aura Microwave Limb Sounder (MLS) [18]. We use the monthly mean data at the 1°×1.25° horizontal resolution from October 2004 to December 2015 (data available at https://acd-ext.gsfc.nasa.gov/Data_services/cloud_slice/new_data.html). Both the GOME-OMI and OMI-MLS datasets have been comprehensively validated by ozonesonde observations [18, 19] and are used for tropospheric ozone trend analyses in the TOAR [8].

2.3. GEOS-Chem simulations

We investigate the tropospheric ozone trends in the SH using GEOS-Chem global three-dimensional chemical transport model (v10-01; http://www.geos-chem.org; [20]) driven by assimilated meteorology from the Modern Era Retrospective–analysis for Research and Applications (MERRA). The MERRA reanalysis has a spatial resolution of 0.667° longitude × 0.5° latitude with 72 vertical layers extending from surface to 0.01 hPa. We downgrade it to 5° longitude × 4° latitude and 47 layers in the vertical for input to GEOS-Chem. The model includes a detailed NO_x–O_x–hydrocarbon–aerosol–bromine tropospheric chemical mechanism [21]. Stratospheric chemistry is simulated using the linearized ozone parameterization (LINOZ) [22]

and using monthly mean production rates and loss frequencies from the Global Modeling Initiative (GMI) model for other stratospheric species [23].

We conduct a standard simulation (BASE) using year-specific meteorology and emissions from 1990 to 2010 as constrained by the availability of anthropogenic emissions and MERRA reanalysis data. Anthropogenic emissions are from the Emissions Database for Global Atmospheric Research (EDGAR v4.2 (http://edgar.jrc.ec.europa.eu/) for 1990–2008; the 2008 emissions are used for years afterwards), and overwritten with regional emission inventories in the Northern Hemisphere (Fig. S1 online). For global biomass burning emissions, we use the Atmospheric Chemistry and Climate Model Intercomparison Project (ACCIMP) biomass burning inventory for years before 1997 and the Global Fire Emission Database version 3 (GFED3) for years 1997–2010. We reduce the 1990–1996 ACCMIP emissions by 30% to correct the bias between these two inventories based on their comparison results for the overlapping years of 1997–2000 following [5]. Climate-sensitive natural emissions of ozone precursors, such as biogenic emissions of non-methane volatile organic compounds (NMVOCs), soil and lightning emissions of NO_x, are calculated online in the model. Methane concentrations in the model are prescribed as uniform and fixed mixing ratios over four latitudinal bands (90°–30°S, 30°S–0°, 0°–30°N, and 30°–90°N), with the year-specific annual mean concentrations constrained by measurements from the NOAA Global Monitoring Division (GMD).

We conduct sensitivity simulations to quantify the contributions to SH tropospheric ozone trends separately from interannual changes in anthropogenic emissions (FEMIS), biomass burning emissions (FBIOB), methane concentration (FCH4), and meteorology (FMET) by fixing a specific source or meteorology at the 1990 conditions in the model simulation. Another sensitivity simulation (FTRANS) is conducted to further separate the influences of dynamics from other meteorological variables (e.g., temperature). This is examined by only fixing horizontal winds and surface pressure (therefore vertical winds) to the year 1990 conditions, while using year-specific conditions for other meteorological variables such as temperature and clouds as the BASE simulation. The contribution of each factor can then be estimated as the difference of ozone trends estimated in the BASE simulation and in the sensitivity simulation. Simulation configurations are

summarized in Table S2 (online). We also conduct model tagged tracer simulations to identify transport of specific sources for the period of 1990–2010. The tagged ozone simulation labels stratospheric ozone (ozone produced in the stratosphere from photolysis of molecular oxygen) as a tagged tracer and simulates its transport in the troposphere [24]. This tagged stratospheric ozone is subject to tropospheric loss using ozone loss frequencies computed in the BASE simulation and thus diagnoses simulated stratospheric contributions to tropospheric ozone.

3. Results

3.1. Observed tropospheric ozone trend in the Southern Hemisphere

Here we summarize ozone concentrations and trends over 1990-2015 derived from available surface monitoring, ozonesonde, and satellite observations in the SH as described in Section 2.1. All nine SH surface sites show increasing annual ozone concentrations with an average trend of 0.10 ± 0.06 ppbv a^{-1} (mean ± standard deviation), and seven of them are statistically significant ($P < 0.10$) (Table 1). Slightly stronger ozone trends are shown in austral autumn (March–April–May, MAM), when all nine surface sites show positive ozone trends and six of them present the largest increasing rates compared with other seasons (on average 0.14 ppbv a^{-1} in MAM compared to 0.07-0.12 ppbv a^{-1} for other seasons, Table 1 and Fig. 1b). Ozonesonde measurements at Lauder and Neumayer also record increasing MAM ozone extends from the surface to the upper troposphere (~10 km over these sites) (Table S3 online). Tropospheric column ozone (TCO) levels show trends of 0.04 ($P < 0.10$) and 0.02 ($P > 0.10$) Dobson Unit (DU) per year over MAM 1990–2015 at the two ozonesonde sites, respectively, slightly larger than those in other seasons. TCO satellite observations from both GOME-OMI and OMI/MLS show increases in TCO over most areas of the SH despite some regional and seasonal differences, demonstrating that the increasing trends are likely widespread in the SH (Fig. S2 online). However, interpreting the absolute magnitudes of satellite observed TCO trends needs cautions [8] because linear trend analyses using OMI datasets can be affected by the instrument row anomaly and retrieval sensitivity [19].

The increases of tropospheric ozone in the SH over 1990-2015 are supported by reported SH tropospheric ozone trends from individual in-situ observations in previous studies. As summarized in Fig 1a and Table S4 (online), nearly all reported records suggested increasing

194 surface/tropospheric ozone from 1990s, except two located in South Africa that likely influenced
195 by local industrial emissions. Ozone trends derived in our study are in general consistent with
196 previous published work (Table S4 online). We also find in Table S3 (online) that the increasing
197 ozone generally does not extend to the lower stratosphere. This is consistent with recent studies
198 showing no significant or decreasing ozone in the lower stratosphere during this period based on
199 merged satellite and ozonesonde observations [7, 25, 26], which can be influenced by climate
200 variability such as ENSO and the Quasi-Biennial Oscillation (QBO) [27]. The observed ozone
201 decreases in the lower stratosphere (12–20 km) at SH mid-latitudes have important implication to
202 quantify the potential large-scale stratospheric ozone impacts as will be discussed in Section 3.7.
203
204 **3.2. Model evaluation**
205 A recent global evaluation of the GEOS-Chem tropospheric ozone simulation using ozonesonde,
206 commercial aircraft, and satellite observation shows no significant model bias in the SH, including
207 for large-scale spatial and seasonal patterns [28]. This is further supported by our evaluation of the
208 BASE simulation using ozone measurements over 1990–2010 described above. We show that the
209 BASE simulation is able to capture spatial and temporal distributions of ozone concentration in the
210 SH (Figs S3-S6 online). Comparisons of measured and simulated monthly mean surface ozone
211 concentrations at the WDCGG surface sites show high correlation coefficients (r = 0.84 for all
212 available monthly data) and small mean biases (−1.2 ppbv). Both measurements and model results
213 show the highest hemispheric mean surface ozone in austral winter (June-July-August, JJA) and
214 minimum in austral summer (December-January-February, DJF) with a high correlation coefficient
215 (r = 0.98, Fig. S4b online). The BASE model reproduces increasing annual ozone concentrations
216 over 1990–2010 at a rate of 0.07±0.02 ppbv a^{-1} averaged for the nine SH surface sites, and shows
217 slightly larger trends in MAM (0.09±0.04 ppbv a^{-1} compared to 0.04-0.08 ppbv a^{-1} for other
218 seasons, Fig. S5 online). Although the model still underestimates observed ozone trends
219 particularly at high SH latitudes (Fig. 2a), it is in notably better agreement with the observations
220 compared with previous climate-chemistry model models that predicted near zero trends at the SH
221 surface sites [2].
222
223 We also compare simulated vertical distributions of ozone concentrations and trends over 1990–

2010 with ozonesonde observations at Neumayer (70.7°S, 8.3°W) and Lauder (45.0°S, 169.7°E) (Fig. S6 online). The model generally captures the vertical ozone structure except for some high biases at Lauder in the upper troposphere. It reproduces the positive trends in tropospheric ozone at Lauder, but fails to capture the negative trends at Neumayer in JJA and DJF. Simulated tropospheric ozone burden within 60°S–60°N averages 320 teragram (Tg) annually, comparable to the range of 281–318 Tg estimated from multiple satellite products [8].

3.3. SH tropospheric ozone trend drivers in MAM

Figure 2 shows observed and simulated MAM mean tropospheric ozone trends and their drivers at the surface sites and averaged over three latitudinal bands in the SH for 1990–2010. Figure S7 and S8 (online) show, respectively, the simulated surface and zonal mean ozone trends for all four seasons. Here we focus on austral autumn (MAM) when the biomass burning influence is lowest and the tropospheric ozone trend is more robust in both observations and simulations (observed trend of 0.15 in MAM compared to 0.11-0.12 ppbv a^{-1} in other seasons, Fig. S5 online), and will discuss other seasons in Section 3.6. Observed surface ozone trends over MAM 1990–2010 range from 0.07 to 0.27 ppbv a^{-1} in the extratropics, with larger trends at high latitudes (90°–60°S, 0.19 ± 0.11 ppbv a^{-1}) than mid-latitudes (60°–30°S, 0.11 ± 0.03 ppbv a^{-1}). The GEOS-Chem simulation shows a widespread distribution of increasing trends in the extratropical SH over MAM 1990–2010. It captures observed increasing SH ozone concentrations with simulated trends of 0.12 ± 0.03 ppbv a^{-1} over 90°–60°S and 0.06 ± 0.03 ppbv a^{-1} over 60°–30°S (Fig. 2a). Trends over the tropics are more variable with decreases found in southern Africa, South America, and southwestern Pacific and increases over other regions (Fig. 2b). Overall the simulated tropospheric ozone burden in the SH (90°–0°S) show increases at 0.10 Tg a^{-1} over MAM 1990–2010.

Sensitivity simulations as described in Section 2.3 allow us to separate influences from emission sources and meteorology. We find in Fig. 2a that changes in meteorology better explain the increasing ozone trends at these SH sites than changes in global emission and CH_4 concentration, and transport is more specifically responsible. For the ensemble of extratropical SH surface sites, changes in transport contribute to trends of 0.10 ± 0.04 ppbv a^{-1}, compared with 0.01 ± 0.01 ppbv a^{-1} from anthropogenic emissions and 0.02 ± 0.00 ppbv a^{-1} from rising CH_4 over MAM 1990–

2010. We find that stratospheric ozone concentration changes due to changes in transport account for about half of simulated trends as shown in Fig. 2a and will be discussed later. Changes in meteorology and particularly transport are also an important driver of the horizontal and vertical distributions of tropospheric ozone trends in the SH for all seasons (Figs S7, S8 online). By contrast, anthropogenic emission changes and rising methane concentrations drive spatially uniform trends in the SH. Biomass burning emissions have larger impact on the spatial distribution of tropical ozone trend over the tropics, yet its contributed ozone presents a slightly negative trend (about −0.01 ppbv a^{-1}) averaged for the extratropics (Figs S7, S8 online).

The lifetime of ozone (more than one month in the free troposphere) allows it to be transported at hemispheric scales. The widespread ozone increases over the extratropical SH contributed by transport as shown in Fig. 2a suggest changes in the meridional circulations as the most likely cause. Figure 3 illustrates the linkage. The meridional circulations including the Hadley circulation can be described by the mean meridional mass stream-function (MMS), a measure of meridional air motion. MMS at a pressure level (ψ_p) is calculated by vertically integrating monthly meridional winds from top of the atmosphere to the pressure level (Holton and Hakim, 2012) and therefore quantifies the sum of northward mass flux above a pressure level. The definition is given as

$$\psi_p = \frac{2\pi a \cos\varphi}{g} \int_0^p [v] \mathrm{d}p,$$

where a is the Earth's radius, g is gravity, φ is latitude, and $[v]$ represents the zonal mean meridional wind. Figure 3a presents the climatology and trend of MMS for austral autumns (MAM) 1990–2010 based on the MERRA assimilated meteorology. Negative MMS values within 30°S–0° representing counter clockwise zonal mean circulation (Fig. 3a) identify the SH Hadley circulation (SHHC), while positive MMS values within 60°–30°S represent the SH Ferrel circulation (SHFC). The strongest air subsidence occurs at 35°–20°S, along the subsiding branch of the SHHC. This is also the location where major stratosphere-to-troposphere transport occurs [29, 30], as seen from the zonal mean ozone climatology (Fig. 3b).

A number of observations have shown poleward expansion of the Hadley circulation or widening

of the tropical belt in recent decades [31-34]. Expansion rates of approximately 0.5°–1.0° latitude decade^{-1} since 1979 have been identified from a variety of metrics and datasets [34]. Robust expansion of the SHHC has been reported and is likely driven by Antarctic stratosphere ozone depletion and tropospheric greenhouse gas forcing [35-39] but also affected by natural climate variability [40]. In Fig. 3a, statistically significant negative MMS trends (P<0.05) in MAM are shown at the edge of the SHHC subsiding branch (40°–25°S), reflecting a broadening of the subsiding branch and thus poleward expansion of the SHHC. Figure 3c shows the trends in zonal mean wind and simulated ozone concentration during MAM 1990–2010. Associated with the SHHC expansion is stronger subsidence of air near the SHHC poleward edge (~40°S) extending from the tropopause to surface, and enhanced southward winds at these latitudes in the lower troposphere. Accordingly, the MAM zonal mean ozone concentrations show statistically significant (P<0.05) increasing trends throughout the troposphere in the extratropical SH. The modelled ozone decreases in the lower stratosphere (12–18 km) (Fig. 3c) are consistent with observations (Section 3.1).

3.4. Mechanism of SH tropospheric ozone increases linked to the SHHC poleward expansion

We explain in Figure 4 that the SHHC poleward expansion, which is also characterized as the widening of the tropics [31, 33, 34], could have enhanced transport of stratospheric ozone to the troposphere in the SHHC subsiding branch, and have also increased tropospheric ozone chemical production by lifting more ozone precursors to the upper troposphere.

To quantify the changes of SHHC, we define the Hadley circulation poleward edge (HCPE) as the latitude where the 500 hPa MMS equals 0 kg s^{-1} that has been widely used in previous studies [32, 37, 41]. We also calculate the 300 hPa downward ozone flux within 50°–30°S as an indicator of ozone input to the extratropical SH from the upper troposphere, where ozone is aggregated from both the stratosphere and the tropics via meridional transport. Figure 4a shows the trend of HCPE over MAM 1990–2010 and its relationships with the seasonal mean downward ozone flux at 300 hPa, total TCO at SH mid-latitudes (60°–30°S), and stratospheric contributed TCO at high latitudes (90°–60°S). The MERRA HCPE values over MAM 1990–2010 decrease (i.e., moving poleward) at a rate of −0.09° per year (P-value < 0.01). This is in the middle of the trends in

HCPE derived from other four reanalysis datasets (−0.07° to −0.14° per year, all with *P*-value < 0.01) (Fig. S9 online). As shown in Fig. 4, HCPE shows significant correlations with 300 hPa downward ozone fluxes (r = −0.90) and with both total and stratospheric TCO (r = −0.63 and −0.51) for MAM 1990–2010. Removing long-term trends in the variables leads to slightly weaker correlation coefficients, reflecting robust linkages between HCPE and TCO in the extratropical SH. Those negative correlations between MAM HCPE and tropospheric ozone concentration are seen throughout the free troposphere of the extratropical SH with the strongest correlations found near the SHHC subsiding branch (Fig. S10 online).

Figure 4 also illustrates how changes in meridional transport associated with poleward expansion of the SHHC affects the ozone distribution in the troposphere. It shows the simulated differences in zonal mean ozone concentrations driven by changes in transport alone (BASE minus FTRANS) as the SHHC moves southward. Values averaged over five years with the lowest HCPE (such as 2009 and 2006) represent the SHHC S-phase condition, and are compared to those averaged over the highest-HCPE years (such as 1992 and 2002; the N-phase condition) during 1990–2010. It can be seen that transport patterns for the S-phase condition lead to 1–5 ppbv higher ozone throughout the SH troposphere (up to 10 ppbv in the upper troposphere) and reduced ozone in the lower stratosphere relative to the N-phase condition.

Extratropical stratosphere-to-troposphere transport in the SH is typically associated with tropopause folds that preferentially occur in the vicinity of subtropical jet streams (about 35°S) and storm tracks (around 50°-60°S) [29, 42]. There is evidence that poleward expansion of the SHHC through modulating the meridional energy flux dynamically shifts the position of storm track poleward [43, 44]. The position of the subtropical jet has also been used to estimate the tropical expansion [33, 34, 45, 46] although the connection between the subtropical jet and the Hadley Circulation expansion remain inconclusive [41]. Poleward expansion of the SHHC can therefore move its subsidence branch and likely the stratosphere-to-troposphere transport occurring areas to higher latitudes. Since ozone concentrations increase sharply with latitudes near the edge of the SHHC (Fig. 3b), it then brings air with higher ozone downward from the stratosphere and at higher latitudes where the lifetime of ozone is longer. As shown in Fig. 4c,

changes in stratospheric ozone dominate tropospheric ozone increases at high latitudes as the SHHC moves poleward.

The SHHC expansion also features a narrowing and strengthening ascending branch as well as a widening subsiding branch [47, 48]. These dynamical changes do not simply redistribute ozone, but affect its chemical production by changing distributions of ozone precursors. The widening of the tropics places more lightning NO_x emissions towards the tropics and in the upper troposphere. It also lifts more CO and peroxyacetylnitrate (PAN; a NO_x reservoir species) over the tropics in the upper troposphere (Fig. S11 online), where high UV radiation and low water vapor conditions favor more ozone to be produced. These redistributions of ozone precursors increase ozone chemical production with the largest enhancements in the middle and upper troposphere of the subtropics (Fig. 4d). We thus propose that both increases in stratospheric ozone influences and tropospheric production lead to the strong correlation between HCPE and 300 hPa downward ozone fluxes (50°–30°S) as seen in Fig 4a.

3.5. Other climate variabilities contributed to ozone trend in the SH tropics

Recent studies have highlighted the influences of climate variability on tropospheric ozone in the NH associated with atmospheric warming and interannual climate variability such as ENSO. We find that these climatic influences mainly contribute to the variable ozone trends over the SH tropics and have smaller impacts at the SH higher latitudes. Changes in temperature alter ozone concentrations by modulating natural precursors emissions such as lightning [23], biogenic emissions [49], biomass burning frequency [50], and also by changing ozone chemistry through photochemical reaction rates, PAN decomposition, and water vapor content in the atmosphere [51, 52], together leading to positive temperature-ozone relationships over continental lands and negative relationships over oceans and remote regions. We show in Figure S12 (online) that temperature-driven biogenic isoprene emission changes are important drivers of surface ozone trends over Africa and South America as seen in Figure 2b.

Furthermore, tropical ozone distribution is highly influenced by ENSO variability [53, 54]. ENSO influences the tropospheric ozone distribution via both chemical and dynamic processes. Under

372 the El Niño condition, abnormal warming over the central-eastern Pacific drives stronger uplifting,
373 which brings ozone-poor air from surface to the upper troposphere (dynamic way), and also lifts
374 moist air leading to faster ozone loss in the free troposphere (chemical way). Opposite influences
375 occur over the western Pacific. This relationship is illustrated by strong negative (positive)
376 correlations between detrended TCO and Niño 3.4 Index (assessed from
377 https://www.esrl.noaa.gov/psd/data/correlation/nina34.data) over the western (eastern) tropical
378 Pacific (Fig. S13 online). Recent studies have pointed out that the Pacific Decadal Oscillation
379 (PDO) is shifting from the positive phase to negative phase around 1998–1999 [4, 55]. This
380 indicates a weakening El Niño impact from early 1990s to 2010, and thus contributes to
381 tropospheric ozone increases over the central-eastern Pacific and decreases over the western
382 Pacific (Fig. 2b and S7 online). Although several studies show that ENSO may affect tropospheric
383 ozone in the extratropical Northern Hemisphere [54], we find weak correlations in the
384 extratropical SH except in DJF (Fig. S13 online).
385
386 **3.6. Ozone trend drivers in other seasons than MAM**
387 The model also reproduces widespread tropospheric ozone increases in other seasons than the
388 austral autumn (MAM) in the extratropical SH. The trends in other seasons are in less statistically
389 significance as also seen from the observations (Table 1 and Fig. S5 online) likely due to larger
390 interannual variability. Changes in transport pattern are also diagnosed as an important driver of
391 the ozone trends (Figs S7 and S8 online). Long-term changes in anthropogenic emissions and
392 methane concentrations contribute more to the SH ozone trends at mid-latitudes in JJA and SON
393 (September-October-November) than MAM and DJF (Figs S7 and S8 online).
394
395 Our results also show some influences of the SHHC poleward expansion on tropospheric ozone
396 distribution in the extratropical SH in these seasons, but are weaker and less statistically
397 significant than MAM (Fig. S10 online). This is likely due to the weaker or insignificant
398 expansion trend of SHHC in these seasons (Fig. S9 online). The MERRA reanalysis indicates the
399 strongest SHHC poleward expansion in MAM, and also significant expansion in DJF, but no
400 trends in JJA (Fig. S9 online). MAM is the only season that all five reanalysis datasets compared
401 in this study present significant HCPE expansions. Although DJF shows significant SHHC

expansion over 1990-2010 from MERRA reanalysis (−0.06° a^{-1}), this season has low stratosphere-to-troposphere transport [30] and strong photochemical loss of ozone in the SH, leading to lower influences of the SHHC poleward expansion than MAM (Fig. S10 online).

3.7 Discussion on possible influences from stratosphere ozone and circulation change

Additional influences can result from recent stratospheric ozone recovery [56] and accelerated stratospheric Brewer–Dobson circulation (BDC) [57, 58]; both may lead to enhanced stratosphere-to-troposphere transport and increase SH tropospheric ozone. Analyses of available evidence suggest that the two effects cannot be the main drivers of SH tropospheric ozone increases in MAM 1990–2010, as indicated by the observed and simulated ozone decreases in the lower stratosphere particularly over 60°S-0° during this period (Section 3.1-3.2). The Antarctic ozone recovery began in 2000 with the largest total ozone column increases over 90°–63°S in September, but insignificant changes in MAM [56]. The small changes or decreases of MAM lower stratospheric ozone in the SH are captured by a climate-chemistry model (CCM) with full stratospheric chemistry [56], and also simulated in our CTM results with the LINOZ mechanism (Fig. 3c).

We thus conclude that stratospheric ozone recovery and strengthening BDC shall not be important drivers of 1990–2010 SH tropospheric ozone increases especially in MAM. This can be further supported by several other studies. Zeng et al. [59] estimated approximately 4–8 ppbv SH tropospheric ozone enhancements (as shown in Fig 1c, b of [59]) if stratospheric ozone would recover from the year 2000 level (total ozone column of ~150 DU at South Pole, estimated from Fig. 1 of ref. [56]) to the 1980s level (~300 DU). This suggests that the flattening stratospheric ozone during 1990–2010 [56] is unlikely to support tropospheric ozone increases of ~0.10 (0.14 in MAM; Table 1) ppbv a^{-1} (about 2–3 ppbv from 1990 to 2010) observed in the period. Using a CCM with full stratospheric chemistry, Hegglin and Shepherd [57] also found no significant change of STE in the SH from 1990 to 2010 (Figure1 in ref. [57]). Their projection showed that changes in stratosphere-to-troposphere ozone flux due to the accelerated BDC showed very slow increase in the SH (0.8% per decade), unlikely to explain the observed trends of 0.15 ppbv a^{-1} (0.56% a^{-1}) in SH troposphere ozone over MAM 1990–2010. The impacts of strengthening BDC

on STE are much stronger in the Northern Hemisphere (NH) and in the future [57].

4. Conclusions and implication

The above analyses all point to a dominant role of changes in meridional circulation driven by poleward expansion of the SHHC particularly in austral autumn (MAM) over 1990-2010. This SHHC poleward expansion associated with its broadening subsiding branch and strengthening ascending branch increases both stratosphere-to-troposphere transport of ozone and tropospheric ozone chemical production, and therefore lead to tropospheric ozone increases in the extratropical SH. This finding explains the inability of climate-chemistry models to reproduce SH tropospheric ozone trends as reported by Cooper et al. [2] and Zeng et al. [7], since the general circulation models consistently underestimate the magnitude of Hadley Circulation poleward expansion [34]. Our results using the MERRA reanalysis generally captures more than or about half of the observed SH ozone trends over this period. The missing part could reflect limitations in the coarse resolution, uncertainties in emission inventory, or other processes not well represented in the model.

Poleward expansion of the Hadley Circulation has also been observed in the NH and partly captured in climate models with anthropogenic forcings [33-35, 37], although some recent studies suggest that the expansion is largely modulated by natural climate variability [40]. We expect a similar impact on NH tropospheric ozone, but to identify it from observations will be difficult due to strong influences from anthropogenic emissions there [3]. Increasing black carbon aerosol and tropospheric ozone are suggested to partly drive the recent Hadley circulation expansion in the NH [37]. Here we find that tropospheric ozone would potentially provide a positive climate feedback. The projection of future changes of the SHHC expansion is somewhat uncertain due to competing effects of increasing greenhouse gases and stratospheric ozone recovery [60]; it thus brings additional uncertainty in our projection of tropospheric ozone changes which deserve more attention in future research.

Conflict of interest

The authors declare that they have no conflict of interest.

Acknowledgments

The work was supported by the National Natural Science Foundation of China (41475112, 41375072, 41530423) and the National Key Research and Development Program of China (2017YFC0210102). Xiao Lu is also supported by the Chinese Scholarship Council. Daniel J. Jacob acknowledges support from the NASA Atmospheric Chemistry Modeling and Analysis Program. We thank Owen. R. Cooper of NOAA Earth System Research Laboratory and Guang Zeng of National Institute of Water and Atmospheric Research for suggestions on the ozone measurements, and Jerry Ziemke of Morgan State University for providing the OMI-MLS dataset. We also acknowledge the Harvard GEOS-Chem Support Team for the model maintenance and development, and all contributors to ozone observations available at the WMO World Data Center of Greenhouse Gas (WDCGG) and the World Ozone and Ultraviolet Radiation Data Centre (WOUDC).

Author contributions

Lin Zhang and Xiao Lu designed the study. Lin Zhang supervised the project. Xiao Lu performed model simulations and conducted analyses with the assistance of Yongyun Hu, Daniel J. Jacob, Yuanhong Zhao, Lu Hu, and Meng Gao. Xiong Liu contributed the satellite ozone products; Irina Petropavlovskikh and Audra McClure-Begley contributed the surface measurements; R.Q. contributed the lauder ozonesonde measurements. Lin Zhang, Daniel J. Jacob, and Xiao Lu wrote the paper. All authors contributed to the interpretation of the results and improvement of the paper.

Reference

[1] Monks PS, Archibald AT, Colette A, et al. Tropospheric ozone and its precursors from the urban to the global scale from air quality to short-lived climate forcer. Atmos Chem Phys, 2015, 15: 8889-8973

[2] Cooper OR, Parrish DD, Ziemke J, et al. Global distribution and trends of tropospheric ozone: an observation-based review. Elementa-Sci Anthrop , 2014, 2: 000029

[3] Zhang Y, Cooper OR, Gaudel A, et al. Tropospheric ozone change from 1980 to 2010 dominated by equatorward redistribution of emissions. Nature Geosci, 2016, 9: 875-879

[4] Lin M, Horowitz LW, Oltmans SJ, et al. Tropospheric ozone trends at Mauna Loa Observatory

tied to decadal climate variability. Nature Geosci, 2014, 7: 136-143
[5] Lu X, Zhang L, Liu X, et al. Lower tropospheric ozone over India and its linkage to the South Asian monsoon. Atmos Chem Phys, 2018, 18: 3101-3118
[6] Oltmans SJ, Lefohn AS, Shadwick D, et al. Recent tropospheric ozone changes – a pattern dominated by slow or no growth. Atmos Environ, 2013, 67: 331-351
[7] Zeng G, Morgenstern O, Shiona H, et al. Attribution of recent ozone changes in the Southern Hemisphere mid-latitudes using statistical analysis and chemistry-climate model simulations. Atmos Chem Phys, 2017, 17: 10495-10513
[8] Gaudel A, Cooper OR, Ancellet G, et al. Tropospheric ozone assessment report: present-day distribution and trends of tropospheric ozone relevant to climate and global atmospheric chemistry model evaluation. Elementa-Sci Anthrop, 2018, 6: 39
[9] Thompson AM, Balashov NV, Witte JC, et al. Tropospheric ozone increases over the southern Africa region: bellwether for rapid growth in Southern Hemisphere pollution? Atmos Chem Phys, 2014, 14: 9855-9869
[10] Liu J, Rodriguez JM, Thompson AM, et al. Origins of tropospheric ozone interannual variation over Réunion: a model investigation. J Geophys Res, 2016, 121: 521-537
[11] Anet JG, Steinbacher M, Gallardo L, et al. Surface ozone in the Southern Hemisphere: 20 years of data from a site with a unique setting in El Tololo, Chile. Atmos Chem Phys, 2017, 17: 6477-6492
[12] Greenslade JW, Alexander SP, Schofield R, et al. Stratospheric ozone intrusion events and their impacts on tropospheric ozone in the Southern Hemisphere. Atmos Chem Phys, 2017, 17: 10269-10290
[13] Balashov NV, Thompson AM, Piketh SJ, et al. Surface ozone variability and trends over the South African Highveld from 1990 to 2007. J Geophys Res, 2014, 119: 4323-4342
[14] Young PJ, Naik V, Fiore AM, et al. Tropospheric Ozone Assessment Report: assessment of global-scale model performance for global and regional ozone distributions, variability, and trends. Elem Sci Anth, 2018, 6: 10
[15] McClure-Begley A, Petropavlovskikh I, Oltmans S, NOAA Global Monitoring Surface Ozone Network 1973-2014. National Oceanic and Atmospheric Administration, Earth Systems Research Laboratory Global Monitoring Division, Boulder, 2014, http://dx.doi.org/10.7289/V57P8WBF
[16] Thompson AM. Southern Hemisphere Additional Ozonesondes (SHADOZ) 1998–2000 tropical ozone climatology 1. Comparison with Total Ozone Mapping Spectrometer (TOMS) and ground-based measurements. J Geophys Res, 2003, 108: 8238
[17] Liu X, Bhartia PK, Chance K, et al. Ozone profile retrievals from the Ozone Monitoring Instrument. Atmos Chem Phys, 2010, 10: 2521-2537
[18] Ziemke JR, Chandra S, Duncan BN, et al. Tropospheric ozone determined from Aura OMI and MLS: Evaluation of measurements and comparison with the Global Modeling Initiative's Chemical Transport Model. J Geophys Res, 2006, 111: D19303
[19] Huang G, Liu X, Chance K, et al. Validation of 10-year SAO OMI Ozone Profile (PROFOZ) product using ozonesonde observations. Atmos Meas Tech, 2017, 10: 2455-2475
[20] Bey I, Jacob DJ, Yantosca RM, et al. Global modeling of tropospheric chemistry with assimilated meteorology: model description and evaluation. J Geophys Res, 2001, 106: 23073-23095
[21] Mao J, Paulot F, Jacob DJ, et al. Ozone and organic nitrates over the eastern United States: sensitivity to isoprene chemistry. J Geophys Res, 2013, 118: 11256-211268
[22] McLinden CA, Olsen SC, Hannegan B, et al. Stratospheric ozone in 3-D models: a simple

chemistry and the cross-tropopause flux. J Geophys Res, 2000, 105: 14653-14665
[23] Murray LT, Logan JA, Jacob DJ. Interannual variability in tropical tropospheric ozone and OH: the role of lightning. J Geophys Res, 2013, 118: 11468-411480
[24] Zhang L, Jacob DJ, Yue X, et al. Sources contributing to background surface ozone in the US Intermountain West. Atmos Chem Phys, 2014, 14: 5295-5309
[25] Steinbrecht W, Froidevaux L, Fuller R, et al. An update on ozone profile trends for the period 2000 to 2016. Atmos Chem Phys, 2017, 17: 10675-10690
[26] Ball WT, Alsing J, Mortlock DJ, et al. Evidence for a continuous decline in lower stratospheric ozone offsetting ozone layer recovery. Atmos Chem Phys, 2018, 18: 1379-1394
[27] Diallo M, Riese M, Birner T, et al. Response of stratospheric water vapor and ozone to the unusual timing of El Niño and the QBO disruption in 2015–2016. Atmos Chem Phys, 2018, 18: 13055-13073
[28] Hu L, Jacob DJ, Liu X, et al. Global budget of tropospheric ozone: evaluating recent model advances with satellite (OMI), aircraft (IAGOS), and ozonesonde observations. Atmos Environ, 2017, 167: 323-334
[29] Stohl A, Bonasoni P, Cristofanelli P, et al. Stratosphere-troposphere exchange: a review, and what we have learned from STACCATO. J Geophys Res-Atmos, 2003, 108: 8516
[30] Škerlak B, Sprenger M, Wernli H. A global climatology of stratosphere-troposphere exchange using the ERA-interim data set from 1979 to 2011. Atmos Chem Phys, 2014, 14: 913-937
[31] Fu Q, Johanson CM, Wallace JM, et al. Enhanced mid-latitude tropospheric warming in satellite measurements. Science, 2006, 312: 1179
[32] Hu Y, Fu Q. Observed poleward expansion of the Hadley Circulation since 1979. Atmos Chem Phys, 2007, 7: 5229-5236
[33] Seidel DJ, Fu Q, Randel WJ, et al. Widening of the tropical belt in a changing climate. Nature Geosci, 2008, 1: 21-24
[34] Lucas C, Timbal B, Nguyen H. The expanding tropics: a critical assessment of the observational and modeling studies.Wires Clim Change, 2014, 5: 89-112
[35]Lu J, Deser C, Reichler T. Cause of the widening of the tropical belt since 1958. Geophys Res Lett, 2009, 36: L03803
[36] Son SW, Gerber EP, Perlwitz J, et al. Impact of stratospheric ozone on Southern Hemisphere circulation change: a multimodel assessment. J Geophys Res, 2010, 115: D00M07
[37] Allen RJ, Sherwood SC, Norris JR, et al. Recent Northern Hemisphere tropical expansion primarily driven by black carbon and tropospheric ozone. Nature, 2012, 485: 350-354
[38] Nguyen H, Lucas C, Evans A, et al. Expansion of the Southern Hemisphere Hadley Cell in response to greenhouse gas forcing. J Clim, 2015, 28: 8067-8077
[39] Hu Y, Huang H, Zhou C. Widening and weakening of the Hadley Circulation under global warming. Sci Bull, 2018, 63: 640-644
[40] Mantsis DF, Sherwood S, Allen R, et al. Natural variations of tropical width and recent trends. Geophys Res Lett, 2017, 44: 3825-3832
[41] Davis N, Birner T. On the discrepancies in tropical belt expansion between reanalyses and climate models and among tropical belt width metrics. J Clim, 2017, 30: 1211-1231
[42] Shaw TA, Baldwin M, Barnes EA, et al. Storm track processes and the opposing influences of climate change. Nature Geosci, 2016, 9: 656-664
[43] Yin JH. A consistent poleward shift of the storm tracks in simulations of 21st century climate.

582 Geophys Res Lett, 2005, 32: L18701
583 [44] Mbengue C, Schneider T. Linking Hadley Circulation and storm tracks in a conceptual model of
584 the atmospheric energy balance. J Atmos Sci, 2018, 75: 841-856
585 [45] Archer CL, Caldeira K. Historical trends in the jet streams. Geophys Res Lett, 2008, 35: L08803
586 [46] Ivy DJ, Hilgenbrink C, Kinnison D, et al. Observed changes in the southern hemispheric
587 circulation in May. J Clim, 2017, 30: 527-536
588 [47] Lau WK, Kim KM. Robust Hadley Circulation changes and increasing global dryness due to CO_2
589 warming from CMIP5 model projections. Proc Natl Acad Sci USA, 2015, 112: 3630-3635
590 [48] Su H, Jiang JH, Neelin JD, et al. Tightening of tropical ascent and high clouds key to precipitation
591 change in a warmer climate. Nat Commun, 2017, 8: 15771
592 [49] Fu T M, Zheng Y, Paulot F, et al. Positive but variable sensitivity of August surface ozone to
593 large-scale warming in the southeast United States. Nat Clim Change, 2015, 5: 454-458
594 [50] Lu X, Zhang L, Yue X, et al. Wildfire influences on the variability and trend of summer surface
595 ozone in the mountainous western United States. Atmos Chem Phys, 2016, 16: 14687-14702
596 [51] Jacob DJ, Winner DA. Effect of climate change on air quality. Atmos Environ, 2009, 43: 51-63
597 [52] Doherty RM, Wild O, Shindell DT, et al. Impacts of climate change on surface ozone and
598 intercontinental ozone pollution: a multi-model study. J Geophys Res, 2013, 118: 3744-3763
599 [53] Oman LD, Ziemke JR, Douglass AR, et al. The response of tropical tropospheric ozone to ENSO.
600 Geophys Res Lett, 2011, 38: L13706
601 [54] Olsen MA, Wargan K, Pawson S. Tropospheric column ozone response to ENSO in GEOS-5
602 assimilation of OMI and MLS ozone data. Atmos Chem Phys, 2016, 16: 7091-7103
603 [55] Kosaka Y, Xie SP. Recent global-warming hiatus tied to equatorial pacific surface cooling. Nature,
604 2013, 501: 403-407
605 [56] Solomon S, Ivy DJ, Kinnison D, et al. Emergence of healing in the Antarctic ozone layer. Science,
606 2016, 353: 269-274
607 [57] Hegglin MI, Shepherd TG. Large climate-induced changes in ultraviolet index and
608 stratosphere-to-troposphere ozone flux. Nature Geosci, 2009, 2: 687-691
609 [58] Butchart N. The Brewer-Dobson circulation. Rev Geophys, 2014, 52: 157-184
610 [59] Zeng G, Morgenstern O, Braesicke P, et al. Impact of stratospheric ozone recovery on tropospheric
611 ozone and its budget. Geophys Res Lett, 2010, 37: L09805
612 [60] Perlwitz J. Atmospheric science: tug of war on the jet stream. Nat Clim Change, 2011, 1: 29-31
613

Figure Captions

Figure 1 | Tropospheric ozone trends from the 1990s to 2015 in the Southern Hemisphere (SH). a, a summary of observed ozone trends in the SH from recent publications. Circles denote ground observations and squares denote ozonesonde observations in the lower or middle troposphere. See Table S1 (online) for references and details. **b,** Observed austral autumn mean ozone concentrations at nine surface sites, tropospheric column ozone (TCO) at two sonde sites, and satellite observed TCO from GOME-OMI and OMI/MLS over 1990–2015 (Supplementary Information 1) grouped into three SH latitudinal bands (90°–60°S, 60°–30°S, and 30°S–0°). Filled symbols denote surface concentrations in unit of ppbv (left axes), and open circles denote TCO values in unit of DU (right axes). Solid and dashed lines represent statistically significant (at 90% confidence level) and insignificant linear trends, respectively. **c**, Ozonesonde trends in austral autumn at Lauder (grey) and Neumayer-S (green). Horizontal bars are standard deviations.

Figure 2 | Drivers of the tropospheric ozone trends in March–April–May (MAM) from the 1990s to 2010 in the SH. Observed trends (black bars) are compared with the BASE simulated results (red bars) at nine surface sites (circles in the right panel, A–I) averaged to three latitudinal bands. Also shown are contributions to the simulated trend from long-term changes in transport patterns (TRANS; blue bars), stratospheric ozone influences (STRAT; green bars), anthropogenic emissions (EMIS; orange bars), global methane levels (CH_4; purple bars), and biomass burning emissions (BIOB; grey bars) (Methods). Grey horizontal bars denote standard deviations over sites. The right panel shows the spatial distribution of surface ozone trends from the BASE simulation. Black dots denote statistically significant ($P < 0.05$). Pluses (J–K) denote the two sonde sites.

Figure 3 | Linkage between changes in meridional circulations and tropospheric ozone in the SH over MAM 1990–2010. a, 1990–2010 climatological mean (black contours) and trends (filled contours) of the mean meridional mass stream-function (MMS). Positive MMS values represent clockwise meridional circulation and vice versa. **b**, Simulated zonal mean ozone concentrations averaged over MAM 1990–2010. Also shown are climatological zonal mean winds (vectors). **c**, Corresponding trends of zonal mean simulated ozone and meridional wind (vectors). The white line denotes the climatological MAM tropopause. Stippling in **a** and **c** denotes statistically significant ($P < 0.05$).

Figure 4 | Stronger stratosphere-to-troposphere transport and chemical production of ozone associated with poleward expansion of the SH Hadley Circulation (SHHC) over MAM 1990–2010. a, The SHHC Poleward Edge (HCPE; negative bars in blue represent poleward anomalies), downward ozone flux at 300 hPa averaged over the mid-latitudes (50°–30°S) (red line; downward flux is defined as positive), TCO averaged within 60°–30°S from the BASE simulation (purple line),

and stratospheric ozone contribution from the tagged simulation averaged within 90°–60°S (green lines). Values are anomalies relative to MAM 1990–2010. The HCPE expansion rate, correlation coefficients (*r*) of HCPE with downward ozone flux, TCO, and stratospheric ozone contribution (with and without trends) are shown inset. **b**, Differences in zonal mean ozone concentration (contours) and wind (vectors) between the HCPE S-phase and N-phase driven by changes in transport (calculated as differences between the BASE and FTRANS simulations; see Methods). The white line denotes the climatological MAM tropopause. **c**, same as **b**, but for stratospheric ozone contributions (see Methods). **d**, same as **b** but for ozone production rates (P_{O3}).

Table 1. Observed annual and seasonal mean surface ozone concentrations and trends in the SH over 1990–2015[a)]

Site		Annual	MAM	JJA	SON	DJF
Tutuila (12.2°S)	mean	13.70±1.00	10.83±1.53	18.73±1.93	15.17±2.30	9.96±1.15
	trend	0.07±0.05* (0.51%)	0.04±0.08 (0.41%)	0.13±0.08* (0.69%)	0.13±0.11*,b) (0.88%)	0.02±0.06 (0.47%)
El Tololo (30.2°S)	mean	32.00±1.26	28.60±1.91	32.81±1.33	37.55±1.80	28.71±1.35
	trend	0.11±0.09* (0.35%)	0.20±0.13*,b) (0.70%)	0.14±0.08* (0.42%)	0.11±0.13 (0.30%)	0.07±0.11 (0.24%)
Cape point (34.3°S)	mean	24.30±1.05	23.40±1.23	29.42±1.13	26.97±1.39	17.11±1.21
	trend	0.11±0.04* (0.46%)	0.12±0.04*,b) (0.53%)	0.10±0.05* (0.35%)	0.10±0.06* (0.36%)	0.10±0.05* (0.60%)
Cape grim (40.7°S)	mean	24.96±0.79	24.18±1.09	30.22±0.85	27.67±1.24	17.73±0.89
	trend	0.09±0.02* (0.36%)	0.12±0.03*,b) (0.48%)	0.08±0.03* (0.26%)	0.10±0.05* (0.38%)	0.07±0.04* (0.38%)
Baring head (41.4°S)	mean	21.38±1.60	20.27±1.95	26.24±1.81	23.60±2.68	15.18±1.09
	trend	0.04±0.09 (0.17%)	0.09±0.10b) (0.42%)	−0.00±0.10 (-0.01%)	0.07±0.15 (0.30%)	0.02±0.07 (0.12%)
Syowa (69.0°S)	mean	25.19±0.93	25.18±1.17	32.03±1.48	26.31±1.27	17.16±0.79
	trend	0.08±0.07* (0.31%)	0.11±0.07* (0.43%)	0.16±0.10*,b) (0.49%)	0.10±0.10* (0.38%)	-0.01±0.06 (-0.04%)
Neumayer-G (70.7°S)	mean	24.27±1.49	24.61±1.46	31.42±1.89	24.67±1.58	15.62±1.36
	trend	0.05±0.07 (0.22%)	0.08±0.08* (0.32%)	0.12±0.09* (0.38%)	0.13±0.07*,b) (0.52%)	0.05±0.07 (0.29%)
Arrival heights (77.8°S)	mean	25.92±1.51	25.89±2.09	33.87±1.53	27.29±1.67	16.69±1.68
	trend	0.21±0.09* (0.81%)	0.26±0.11*,b) (0.99%)	0.21±0.09* (0.61%)	0.20±0.11* (0.73%)	0.18±0.12* (1.08%)
South Pole (90°S)	mean	28.40±1.66	25.23±2.10	33.46±1.64	30.67±1.90	24.34±2.09
	trend	0.17±0.05* (0.61%)	0.21±0.06*,b) (0.81%)	0.14±0.06* (0.43%)	0.19±0.06* (0.62%)	0.12±0.09* (0.51%)
Averaged trend[c)]		0.10±0.06 (0.42%)	0.14±0.07b) (0.56%)	0.11±0.06 (0.40%)	0.12±0.04 (0.49%)	0.07±0.06 (0.38%)

a) Mean surface ozone concentrations ± standard deviations are in unit of ppbv, trends ± 90% confidence level are in unit of ppbv a^{-1}, and * denotes statistically significant trends (P-value < 0.1); b) the largest seasonal trend for each site; c) standard deviation of ozone trends over the nine surface sites.

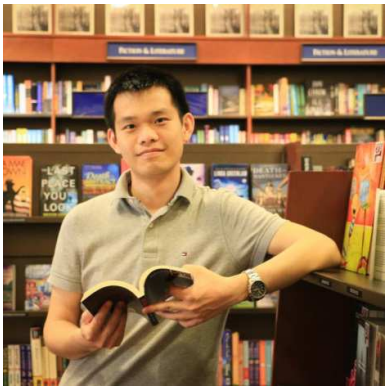

Xiao Lu received his B.S. from the Sun Yat-Sen University in 2014. He is currently a Ph.D. candidate supervised by Prof. Lin Zhang in Department of Atmospheric and Oceanic Sciences, Peking University, China. His research interests mainly focus on tropospheric ozone variabilities and the interactions with climate change.

Lin Zhang received his B.S. from Peking University in 2004, and Ph.D. from Harvard University in 2009. He is presently a tenured associated professor in the Department of Atmospheric and Oceanic Sciences, School of Physics, Peking University. His research aims to better understand the sources, transformation, and sinks of air pollution, as well as its environmental and climatic effects.

Yongyun Hu is a Professor in the Department of Atmospheric and Oceanic Sciences, School of Physics, Peking University. He has broad research interests in present, past, and planetary climates. Yongyun Hu received his B.S. from Sun Yat-sen University,

M.S. from Texas A&M University, and Ph.D. from the University of Chicago. He had worked as a postdoctoral scientist at the University of Washington as well as Columbia University and NASA-GISS.

Daniel J. Jacob is the Vasco McCoy Family Professor of Atmospheric Chemistry and Environmental Engineering at Harvard University. He joined Harvard in 1985 after he received his Ph.D. from Caltech. His research focuses on understanding the chemical composition of the atmosphere, its perturbation by human activity, and the implications for climate change and life on Earth. He has more than 400 peer-reviewed publications and 60,000 citations.

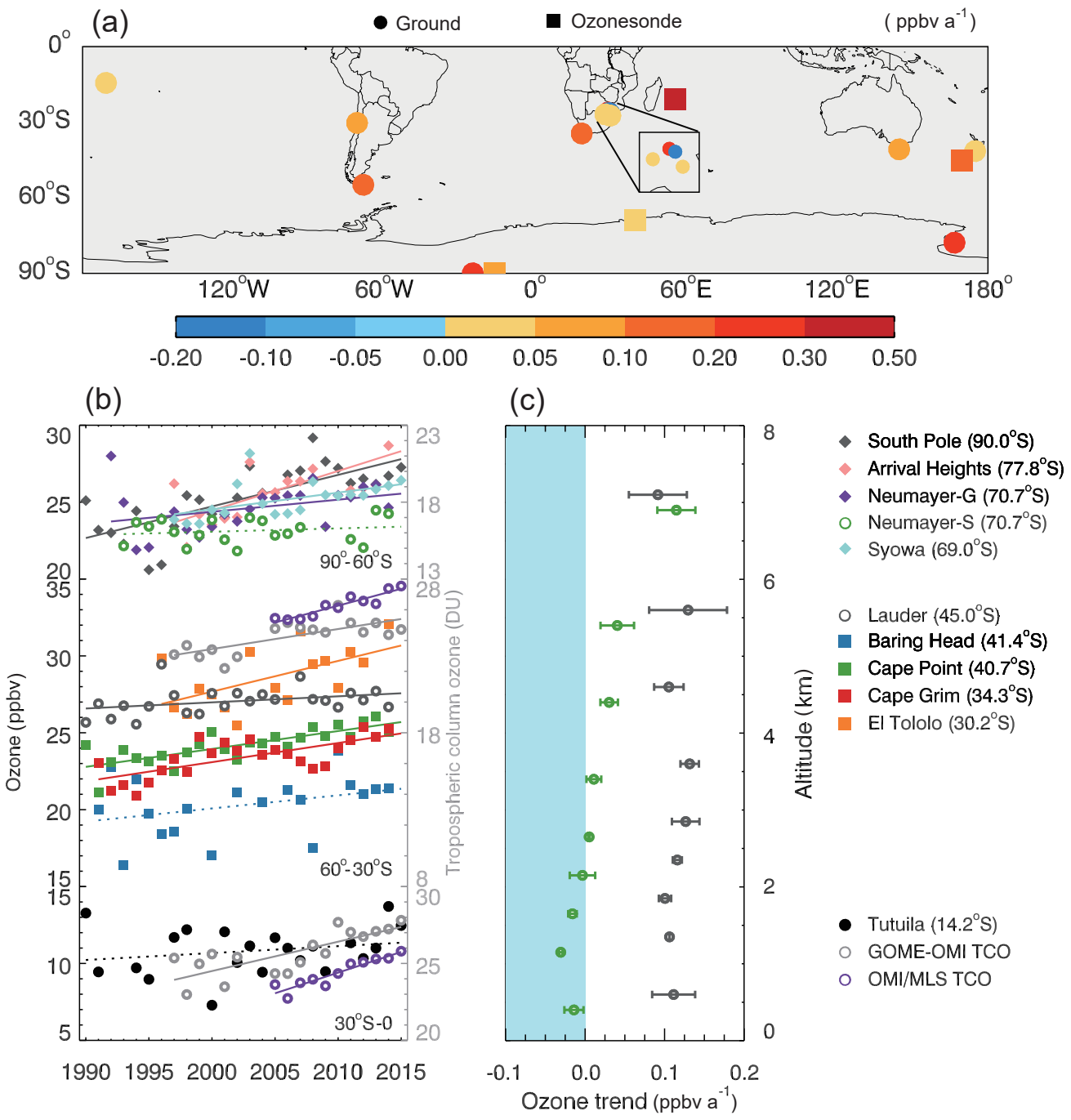
(a)
Ground
Ozonesonde
(ppbv a-1)
0°
30°S
60°S
90°S
120°W
60°W
0°
60°E
120°E
180°
-0.20
-0.10
-0.05
0.00
0.05
0.10
0.20
0.30
0.50
(b)
Ozone (ppbv)
Tropospheric column ozone (DU)
90°-60°S
60°-30°S
30°S-0
1990
1995
2000
2005
2010
2015
(c)
Altitude (km)
Ozone trend (ppbv a-1)
-0.1
0.0
0.1
0.2
South Pole (90.0°S)
Arrival Heights (77.8°S)
Neumayer-G (70.7°S)
Neumayer-S (70.7°S)
Syowa (69.0°S)
Lauder (45.0°S)
Baring Head (41.4°S)
Cape Point (40.7°S)
Cape Grim (34.3°S)
El Tololo (30.2°S)
Tutuila (14.2°S)
GOME-OMI TCO
OMI/MLS TCO

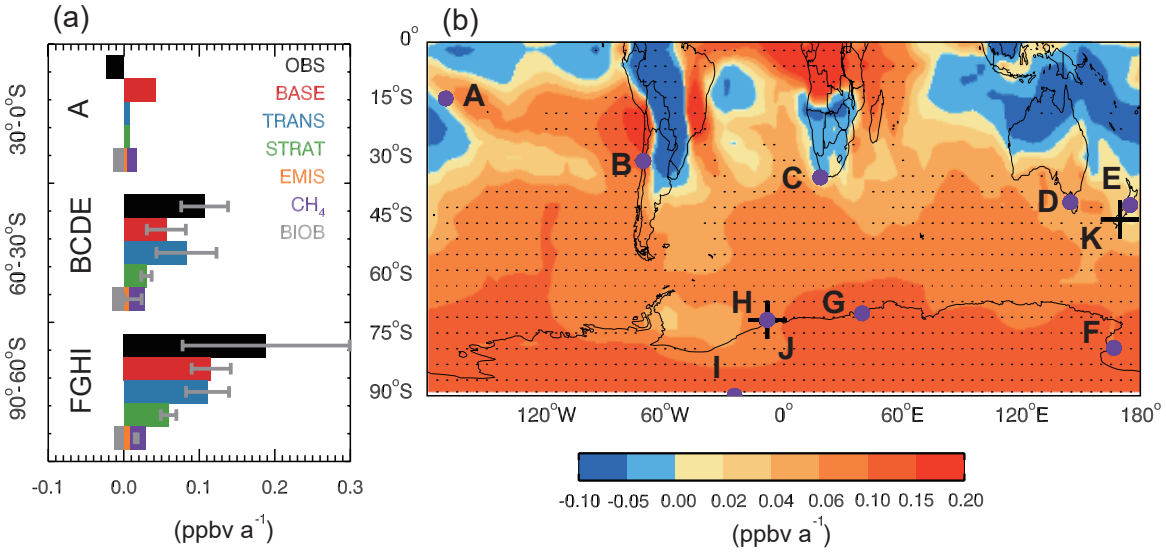
(a)
OBS
BASE
TRANS
STRAT
EMIS
CH4
BIOB
A
BCDE
FGHI
30°-0°S
60°-30°S
90°-60°S
-0.1
0.0
0.1
0.2
0.3
(ppbv a-1)
(b)
0°
15°S
30°S
45°S
60°S
75°S
90°S
120°W
60°W
0°
60°E
120°E
180°
A
B
C
D
E
K
F
G
H
I
J
-0.10 -0.05 0.00 0.02 0.04 0.06 0.10 0.15 0.20
(ppbv a-1)

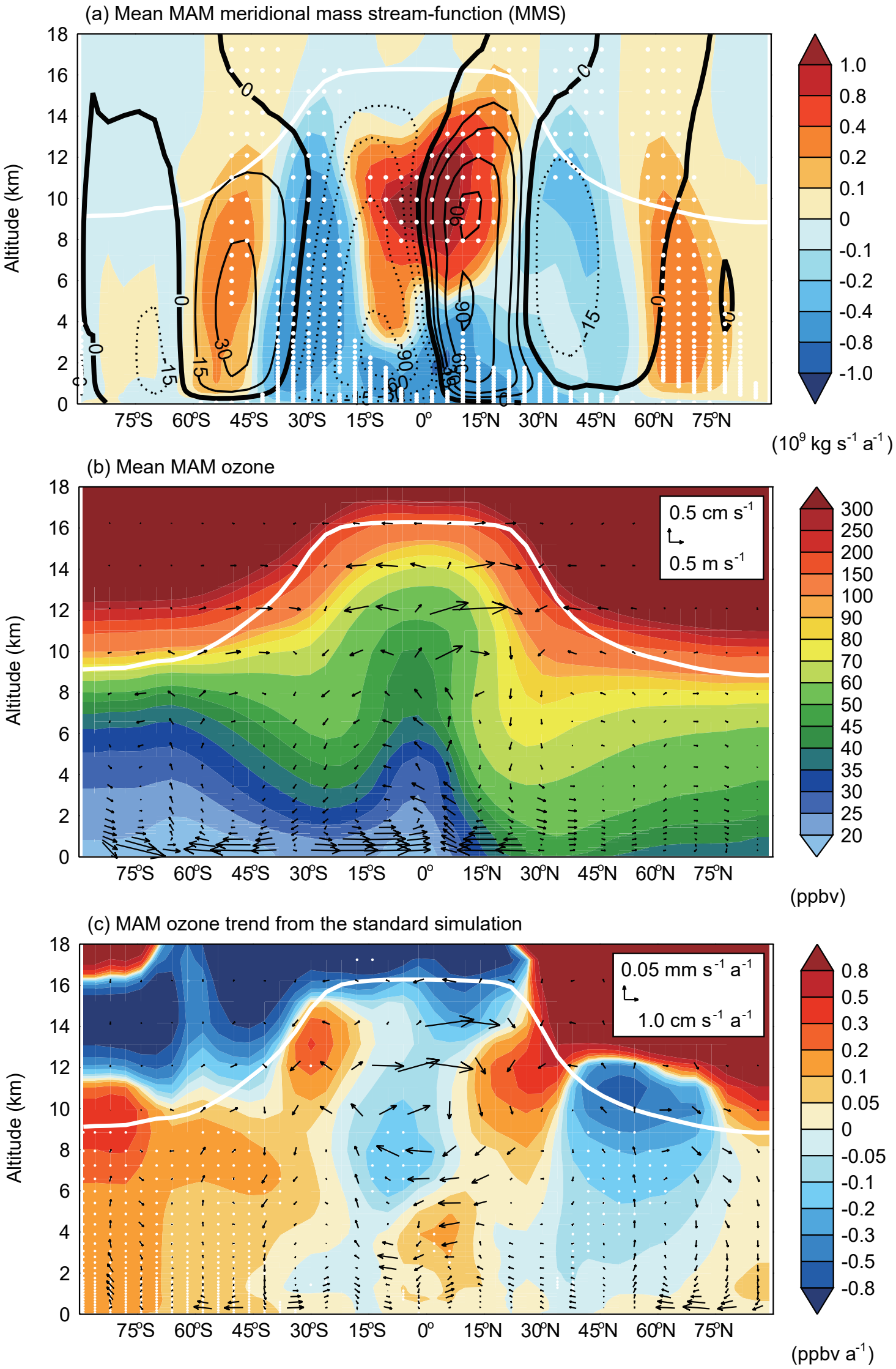
(a) Mean MAM meridional mass stream-function (MMS)
Altitude (km)
18
16
14
12
10
8
6
4
2
0
75°S 60°S 45°S 30°S 15°S 0° 15°N 30°N 45°N 60°N 75°N
1.0
0.8
0.4
0.2
0.1
0
-0.1
-0.2
-0.4
-0.8
-1.0
(10^9 kg s^-1 a^-1)
(b) Mean MAM ozone
Altitude (km)
0.5 cm s^-1
0.5 m s^-1
300
250
200
150
100
90
80
70
60
50
45
40
35
30
25
20
(ppbv)
(c) MAM ozone trend from the standard simulation
Altitude (km)
0.05 mm s^-1 a^-1
1.0 cm s^-1 a^-1
0.8
0.5
0.3
0.2
0.1
0.05
0
-0.05
-0.1
-0.2
-0.3
-0.5
-0.8
(ppbv a^-1)

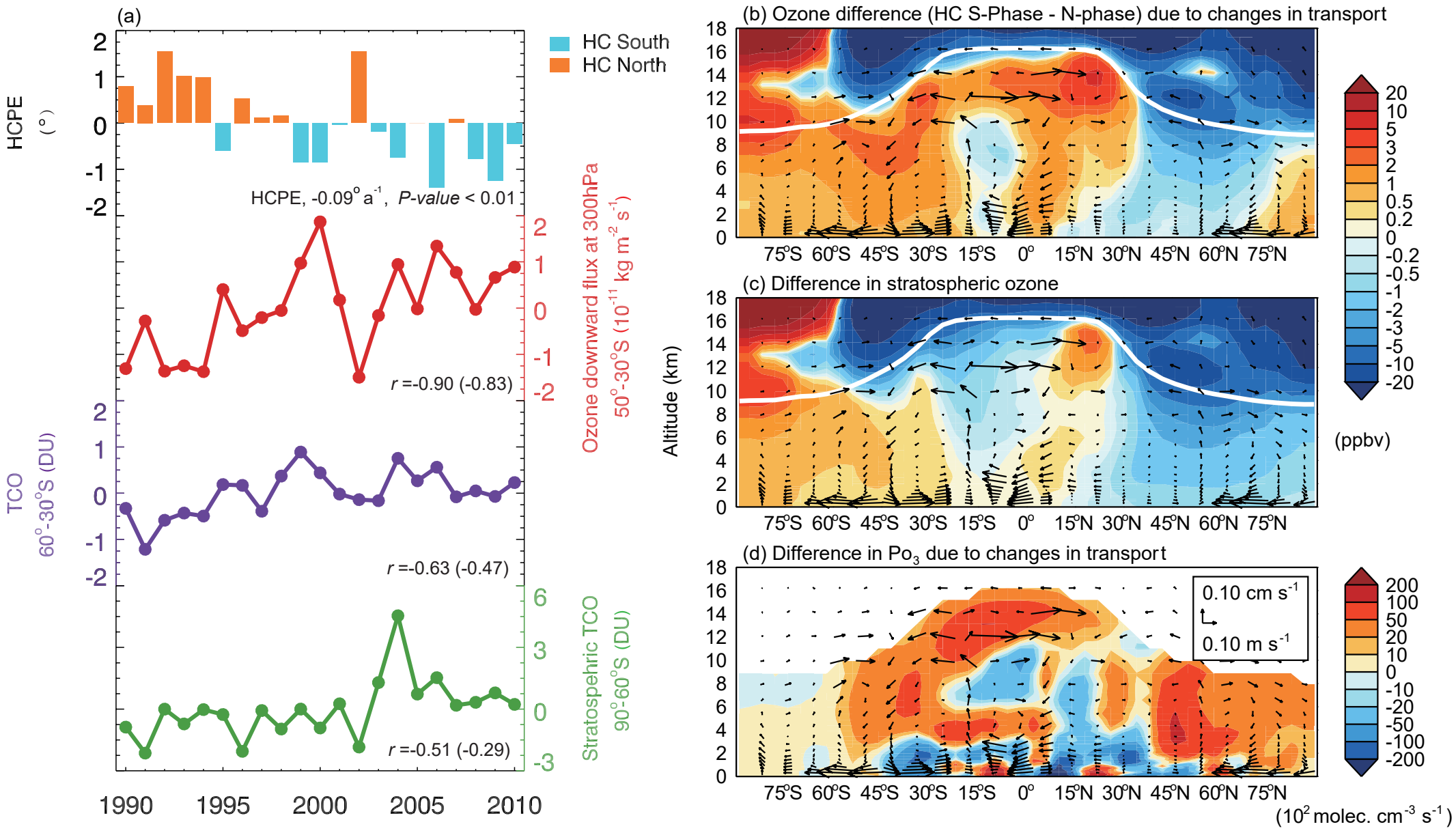
(a)
HC South
HC North
HCPE
(°)
HCPE, -0.09° a-1, P-value < 0.01
r =-0.90 (-0.83)
Ozone downward flux at 300hPa
50°-30°S (10-11 kg m-2 s-1)
TCO
60°-30°S (DU)
r =-0.63 (-0.47)
r =-0.51 (-0.29)
Stratospehric TCO
90°-60°S (DU)
1990
1995
2000
2005
2010
(b) Ozone difference (HC S-Phase - N-phase) due to changes in transport
(c) Difference in stratospheric ozone
Altitude (km)
75°S 60°S 45°S 30°S 15°S 0° 15°N 30°N 45°N 60°N 75°N
(ppbv)
(d) Difference in Po3 due to changes in transport
0.10 cm s-1
0.10 m s-1
(10² molec. cm-3 s-1)